Past Methane Release Events and Environmental Conditions at the Upper Continental Slope of the South China Sea: Constraints by Seep Carbonates

Citation	Han, X., E. Suess, V. Liebetrau, A. Eisenhauer, Y. Huang 2014. Past methane release events and environmental conditions at the upper continental slope of the South China Sea: constraints by seep carbonates. Int J Earth Sci (Geol Rundsch) (2014) 103:1873–1887; DOI 10.1007/s00531-014-1018-5
DOI	10.1007/s00531-014-1018-5
Publisher	Springer
Version	Accepted Manuscript
Terms of Use	http://cdss.library.oregonstate.edu/sa-termsofuse

Past Methane Release Events and Environmental Conditions at the Upper Continental Slope of the South China Sea: Constraints from Seep Carbonates

Xiqiu Han (1)*, Erwin Suess (2, 3), Volker Liebetrau (2), Anton Eisenhauer (2) Yongyang Huang (4)

(1) Key Laboratory of Submarine Geosciences & The Second Institute of Oceanography, State Oceanic Administration, Hangzhou 310012, China

(2) Helmholtz Centre for Ocean Research Kiel (GEOMAR), 24148 Kiel, Germany

(3) College of Earth, Ocean and Atmospheric Sciences, Oregon State University, Corvallis OR 97330, USA

(4) Guangzhou Marine Geological Survey, Guangzhou 510075, China

Corresponding author:

Xiqiu HAN email: xqhan@sio.org.cn Tel: (86) 571 81963004; Fax: (86) 571 88080507

Abstract Authigenic carbonates and chemosymbiotic biota are archives of seepage history and record paleo-environmental conditions at seep sites. Based on mineral and stable isotope compositions and U/Th-isotope systematics of seep carbonates and *Calyptogena* sp shell fragments from three seep sites located at 22°02' ~22°09'N, 118°43'~118°52'E (water depths: 473 m to 785 m) in the northeastern slope of the South China Sea, we obtained the timing of past methane release events and identified samples formed in contact with bottom seawater with negligible pore water influence, largely aragonitic chemoherm samples and shells, to reconstruct the palaeo-bottom water temperatures during their formation. Our results show that all methane release events occurred between 11.5±0.2 ka and 144.5±12.7 ka, when sealevels were about 62 m to 104 m lower than today. The enhanced methane release during low sealevel stands is thought to be a modulating on reduced hydrostatic pressure, increased incision of canyons and the increase of sediment loading. The calculated past bottom water temperatures at one site (Site 3; water depth: 767 m to 771 m) during the periods of low sealevel stands between 11.5 ka and 65 ka were in the range of ~3.3 ºC to ~4.0 ºC, that is ~1.3 ºC to ~2.2 ºC colder than at present. The reliability of $\delta^{18}O$ of seep carbonates and vent bivalve shells as a proxy for bottom water temperatures is critically assessed in light of seepage ^{18}O-enriched fluids from gas hydrate and/or clay dehydration water. Our approach provides for the first time an independent estimate of past bottom water temperatures of the upper continental slope of the South China Sea.

Keywords Seep carbonates; U/Th ages; methane release events; Oxygen isotope; bottom water temperature reconstruction; South China Sea

Introduction

Authigenic carbonates and chemosynthesis-based communities are common manifestations of gas emission and fluid seepage at cold seep sites on active and passive continental margins (Greinert et al. 2010; Roberts and Boland, 2010; Suess, 2010). They provide important information on the nature and origin of fluid source (e.g. Aloisi et al. 2000; Han et al. 2004; Chen et al. 2007; Feng et al. 2009; Han et al. 2013), as well as the environmental conditions (e.g. Teichert et al. 2003; Ge et al. 2010). The limited age data available so far indicate that most seep carbonates tend to form during the periods of low sealevel stands, presumably caused by more intense methane venting due to hydrostatic pressure reduction (Lalou et al. 1992; Aharon et al. 1997; Teichert et al. 2003; Watanabe et al. 2008;

Kutterolf et al. 2008; Bayon et al. 2009; Kiel, 2009; Liebetrau et al. 2010; Feng et al. 2010; Tong et al. 2013). However, authigenic carbonates also form presently at high sealevel, believed to be related to methane release controlled by faulting and fracturing in certain regimes caused by sedimentary loading, salt diapirism and subduction tectonics (e.g. Aharon et al. 1997; Teichert et al. 2003; Chen et al. 2007; Kutterolf et al. 2008; Torres et al. 2009; Liebetrau et al. 2010; Feng et al. 2010).

In 2004, three sites of authigenic seep carbonate fields were discovered on the NE passive margin slope of the South China Sea at water depths between 473-785 m (Suess et al. 2005) (Fig. 1). Our previous studies and subsequent investigations by others have shown that the types of carbonates vary from chemoherm carbonates and crusts that formed on the seafloor and assorted morphologies of chimneys and concretions that formed in the sediments (Han et al. 2008). Anaerobic microbial oxidation of methane (AOM) is responsible for their formation as has been amply documented (Han et al. 2008; Birgel et al. 2008; Yu et al. 2008). The precipitating fluid of chimneys and concretions are ^{18}O-enriched and thought to be associated with gas hydrate dissociation (Chen et al. 2012; Han et al. 2013). However, questions remain about when these carbonates formed and whether or not the oxygen-isotope compositions of chemoherm carbonates and crusts that formed at the seafloor were in equilibrium with seawater and may be used as proxy to recontruct the past bottom water temperatures during their formation. Accordingly, here we (1) provide absolute U/Th ages for the carbonates and associated chemosymbiotic bivalve shells to constrain the timing of past methane release events and their relationship to global sealevel change; (2) calculate the equilibrium temperatures of the carbonates formed at the seafloor to attempt an independent estimate of past bottom water temperatures. The results show when the methane release events occurred and provide some information on how the intermediate water mass of the South China Sea responded to global climate change.

Figure 1 here

Regional setting and sampling sites

The South China Sea is bordered on three sides by passive continental margins and to the east by an active continental margin. The west-advancing accretionary complex off Taiwan Island impinges obliquely onto the

northern continental slope overriding the eastward-dipping subduction zone of the Manila Trench (Lin et al 2008). Since the cessation of the sea floor spreading ~15.5 Ma ago (Briais et al. 1993), the South China Sea has been subject to tectonic subsidence, receiving large amounts of sediments with maximum thickness of Cenozoic deposits exceeding 10 km (Pang et al. 2004). Sediment cores collected during ODP Leg 184 reveal that the sedimentation rate at Site 1144 (20°03' N, 117°25' E, water depth 2037 m) in recent ~1 Ma was as high as 49 cm/ka, with 60% to 70% terrigenous clastics (Wang et al. 2000). Normal faults concentrated beneath the shelf-slope break and overlying the Oligocene breakup unconformity provide conduits for gas and fluid derived from the compaction of the rapidly accumulating sediments to migrate upward and escape to the seafloor (Liu et al. 1997; Ding et al. 2004; Lin et al 2008). The upper slope of the South China Sea is characterized by abundant submarine canyons, gullies and remnant ridges formed by powerful down-cutting turbidity currents whereas the distal slope shows subdued topography and extensive depositional features (Lin et al 2008) (Fig. 1). The water mass of the South China Sea is strongly influenced by cold and saline western Pacific water and warm equatorial Indian Ocean water. During glacial periods, the maximum sealevel was about 123±2 m lower than today (Hanebuth et al. 2009). As a consequence several passages in the south and southeast were closed and most of the shelf area was exposed. Bashi Strait (sill depth ~2400 m) between Taiwan Island and the Philippine Islands was the only passage connecting the South China Sea with the western Pacific Ocean (Wang, 1999).

The study area is located at the transition zone between its passive northern margin and the accretionary eastern margin (Fig. 1). Three fields of seep carbonates on two adjacent ridges were discovered and mapped during RV SONNE Cruise 177 (June-July, 2004). Site 1 (22°09' N, 118°52'E) is located on a mound at water depths between 473 m to 498 m. Site 2 (22°08' N, 118°43' E) is located slightly to the west at water depths between 530 m to 560 m and Site 3 (22°02' N, 118°46' E) to the south at water depths between 765 m to 785 m. Data collected with a deep-towed ocean floor observation system (OFOS) show that the current bottom water temperatures for Sites 1, 2 and 3 were 9.3 to 9.5°C, 7.5 to 7.8°C and 5.3 to 5.6°C and their salinities were 34.39, 34.41 and 34.45 psu, respectively (Suess et al. 2005).

Figure 2 here

Site 1 is dominated by carbonate chimneys, crusts and blocky carbonates. The chimneys are usually 4 cm to 6 cm in diameter and 10 cm to 12 cm long, with an open central channels ~2.5 cm in diameter. Most of chimneys occur on the seafloor at random orientations, indicating that they originally grew in the sediment and later were exhumed and toppled by the currents. Site 2 is characterized by carbonate chimneys protruding from the sediment. They are 8 cm to 40 cm long and 4 cm to 10 cm in diameter, generally bigger and longer compared to those from Site 1 but otherwise of similar morphologies. Site 3 is characterized by abundant disarticulated shells and shell fragments of seep dwelling chemosymbiotic bivalves, a large chemoherm carbonate buildup ("Jiulong Methane Reef"), and carbonate chimneys and concretions (Suess et al. 2005; Han et al. 2008). Methane concentration profiles of the water column show that Site 3 is still weakly active, whereas the other sites seem extinct (Suess et al. 2005). To the west of the study area, seep carbonates were also found in Shenhu area at water depth between 350 m to 400 m (Lu et al. 2006), an area where gas hydrates were successfully recovered from depths between 153 m to 225 m below sea floor at 19.9ºN, 115.2ºE (Zhang, 2007). To the east of study area, a vigorously venting methane seep site was discovered at 22°07' N, 119°17' E water depth of 1125 m (Site F) in 2007 during the NT07-05 cruise (Liu et al. 2008; Morita et al. 2009).

Materials and methods

Seep carbonate samples were collected at Site 1 (TVG 1, 2, 3), Site 2 (TVG 13, 14) and Site 3 (TVG 6, 7, 8, 9, 11) using TV-guided grab sampler (Fig. 1). Samples from Site 1 and Site 2 have dark brown Fe–Mn oxide coatings, indicating that they have been exposed to the oxygenated bottom water for some time. At Site 3, some samples have the same dark brown coating, but others appear rather fresh and are of a greenish–gray color. The morphological, petrographic, mineralogical and C, O-isotopic characteristics of 60 seep carbonates and chemoautotrophic bivalve samples from the study area have been reported in detail by Han et al. (2008).

From these previously described samples, representative carbonates from Sites 1, 2 and 3 were selected for this study. The sample types include chimneys, concretions, crusts, chemoherms and *Calyptogena* bivalve shells. A total of 17 subsamples were taken from freshly cut surfaces using a dental drill. Their exact sampling locations are shown

in Figure 3. The carbonate contents were determined using Carlo Erba NA-1500-CNS analyzer with accuracy better than ±1.5 wt-%.

The mineralogy of the samples was determined by standard X-ray diffraction (XRD) analysis using a Philips PW 1820 diffractometer with Cu K-alpha radiation. The mol-percentage of Mg in calcite was calculated from the d [104] lattice-shift using the average of the linear correlation provided by Goldsmith et al. (1961) and Lumsden (1979). The relative weight percentages of high-Mg-calcite (HMC), low-Mg-calcite (LMC), aragonite, and dolomite were calculated using the linear correlation between XRD-intensity and mineral quantity as given by Milliman (1977).

Carbon- and O-isotope ratios were measured on a Finnigan MAT 252 mass spectrometer. CO_2 extraction for $\delta^{13}C$ and $\delta^{18}O$ was carried out with pure H_3PO_4 at 75 °C. Replicate analyses of a laboratory standard show a standard deviation <0.04‰ for $\delta^{13}C$ and <0.05‰ for $\delta^{18}O$. All of the stable isotopic data are reported relative to the VPDB standard.

$\delta^{18}O$ values of carbonates that formed in contact with free bottom water were used to reconstruct the palaeo-bottom water temperature. For this purpose the experimental equation of inorganic aragonite-water fractionation provided by Kim et al. (2007) was used to calculate the equilibrium formation temperatures of these samples:

$$10^3 \ln\alpha_{arg.\text{-}water} = 17.88\,(10^3/T) - 31.14 \quad (1)$$

The above equation was derived using a newly measured acid fractionation factor ($\alpha_{arag\text{-}acid}$ = 1.01063 at 25°C by Kim et al. 2007), whereas traditionally, the value used was 1.01034 (McCrea, 1950). In order to be comparable to other oxygen isotope fractionation equations, a correction of +0.29 was applied to the equation (1):

$$10^3 \ln\alpha_{arg.\text{-}water} = 17.88\,(10^3/T) - 30.85 \quad (2)$$

Where T is temperature in Kelvin and $\alpha_{agar\text{-}water}$ is the fractionation factor between aragonite and water.

For bivalve shell fragments, the equation of Grossman and Ku (1986) derived from aragonitic mollusks was used:

$$T\,(°C) = 21.8 - 4.69\,(\delta^{18}O_{arag.} - \delta^{18}O_{sw}) \quad (3)$$

For samples containing a mixture of aragonite and varying amounts of LMC and HMC, a correction for each mol-% of $MgCO_3$ enriching the ^{18}O by 0.06‰ and the aragonite-calcite oxygen isotope fractionation factors of 0.6‰ was applied according to Tarutani et al (1969).

Uranium-series measurements for U/Th geochronology and isotope systematics were performed on a VG Axiom MC-ICP-MS at GEOMAR. Multi-ion counting (MIC) set up, lab-procedures and methods followed Fietzke et al. (2005); the decay constants used according to Cheng et al. (2000a). For isotope dilution measurements, a combined $^{233}U/^{236}U/^{229}Th$-spike, with stock solutions calibrated for concentration using NIST-SRM 3164 (U) and NIST-SRM 3159 (Th) as combi-spike, calibrated against CRM-145 uranium standard solution (also known as NBL-112A) for U-isotope composition, and against a secular equilibrium standard (HU-1, uranium ore solution) for determination of $^{230}Th/^{234}U$ activity ratio. Whole procedure blanks were around 4 pg for U, 2 pg for ^{232}Th and 0.2 fg for ^{230}Th.

To obtain precise ages, we select clean aragonitic and/or calcitic cements, void fillings and fracture linings of the samples. The ages thus obtained would represent the latest stage of formation of the carbonates. For samples without such pure carbonate minerals, the matrix was used for dating. 11−94 mg samples were prepared for U and Th separation using Eichrom-UTEVA resin under clean laboratory conditions. Each set of element separations was accompanied by runs of aliquots of the HU-1 equilibrium standard solution to verify procedure reproducibility. A methodology depending uncertainty on $^{230}Th/^{234}U$ activity ratios was less than 0.5%. The geochronological uncertainties of pure aragonitic or calcitic sub-samples are mainly caused by the analytical error of individual sample measurements. For those impure samples contained some unsupported ^{230}Th from detrital sediments, the $^{230}Th/^{232}Th$ activity ratios were corrected by 0.75. This value was calculated using the average U and Th content of the upper continental crust (Wedepohl, 1995) and the radioactive equilibrium between ^{238}U and the daughter product ^{230}Th. Their age uncertainties are a combination of analytical error, precision and accuracy of the correction. We introduced a conservative estimate of ± 0.2 for correction of all samples as potential range of changes. The $^{230}Th/^{232}Th$ activity ratios of leachates (cold 2.5 N HNO_3) from samples TVG14-C1-1A ($CaCO_3$ = 49 wt-%) and TVG14-C2-3A ($CaCO_3$ = 80 wt-%) were also measured. Their values are 0.78 ± 0.03 and 0.77 ± 0.03, respectively (Table 1, 2), indicating that the correction factor of 0.75 ± 0.2 for detrital origin Th is reasonable.

Figure 3 here

Results and discussion

Carbonate characteristics

The carbonate lithologies include micrite, pelmicrite, thrombolite to biomicrite. Chemoherms and crusts are mainly cemented by aragonite. Pure aragonite layers precipitated inside fluid channels, along void or fracture surfaces. Carbonate chimneys and concretions are dominated by microcrystalline HMC with traces of proto-dolomite and LMC, containing abundant terrestrial material such as silt-sized quartz and plagioclase.

The carbonate contents, mineralogy, carbon and oxygen isotopic compositions of the samples are listed in Table 1. The carbonate contents of chimney samples range between 38−77 wt-% whereas the other samples are more pure with carbonate contents well exceeding 80 wt-%. All of the seep carbonate samples have very light $\delta^{13}C$ (from −35.7 to −56.6‰ VPDB) indicating that they are methane-derived (Han et al. 2008; Suess, 2010). The different layers of the uncemented shell (TVG8-S1) show $\delta^{13}C$ values between 2.1 to 2.7‰ VPDB, which are close to that of seawater bicarbonate. However, the cemented shells (TVG9-C4-S1, TVG9-C4-S2, and TVG9-C4-S3) cover a large and systematic range of $\delta^{13}C$ values. TVG9-C4-S3 has a $\delta^{13}C$ value of +2.56‰ VPDB indicating that the carbon was mainly derived from seawater. Whereas TVG9-C4-S2 and TVG9-C4-S1 has $\delta^{13}C$ value of −7.8 and −25.1‰ VPDB, respectively. The shift towards lighter values indicates that the bicarbonate available for shell formation might partly contain anaerobically oxidized methane. The $\delta^{18}O$ of the samples are in the range of 2.68 to 4.35‰ VPDB (Table 1), reflecting the combined effects of temperature and $\delta^{18}O$ of the precipitating fluid.

Table 1 here

U-, Th-isotope characteristics

The U-Th isotope systematics for the samples and their $^{230}Th/^{234}U$ ages are shown in Table 2. The U-content of the samples are in the range of 0.38 to 15.76 µg/g. Uranium is highly soluble under oxic conditions but highly insoluble

under reducing conditions (Barnes and Cochran, 1990). The variation of U in the samples reflects the changing redox conditions during their formation. Carbonates formed in suboxic to anoxic condition are expected to have lower U-contents than those formed under oxic condition (Bayon et al. 2009). The fillings of the chimneys from Site 2 have lower U than their rims (0.62 to 1.30 µg/g vs. 1.68 to 5.42 µg/g), indicating that the filling was formed in more anoxic environment than its rim. This is supported by the REE data in that the Ce-anomaly of the filling is more positive than that of the rim (Ge et al. 2010). In contrast, the aragonitic fillings of chimneys from Site 1 have relatively high U (2.49 to 3.74 µg/g). Their values are comparable to those of aragonitic cements of chemoherm samples from Site 3. This indicates that the precipitation likely occurred under oxic or sub-oxic conditions after the chimneys were excavated and exposed at the seafloor.

The shell samples (TVG8-S1, uncemented; TVG9-C4-S3, cemented) contain very low U-concentrations (0.38-0.72 µg/g), even lower than the chimneys that supposedly formed in the sediments under anoxic conditions. In case of the cemented shell fragments, the U-contents vary strongly. TVG9-C4-S3 has the lowest U of 0.64 µg/g, TVG9-C4-S1 and TVG9-C4-S2 contain U 5.81 and 1.88 µg/g, respectively. This phenomenon is probably due to the biologically induced "vital effect" as living clams strongly discriminate against U-inclusion. But after death the outer shell structure may become more open due to degradation of organic compounds and the uranium from the environment would diffuse into the structure. It has been observed that the U-content of fossil shells could be an order of magnitude higher than that of living shells (Kaufman et al. 1996). Therefore, the U-content suggests that cemented shell fragment TVG9-C4-S3 has not been subject to significant alteration, but the other cemented shell fragment samples have been altered in some degree.

The U-isotope values of the samples fall into three categories. Aragonitic cements of chemoherm and shells from Site 3 have $\delta^{234}U_{(T)}$ (initial $\delta^{234}U$) values between 135±3 and 160±6‰, which encompass modern seawater values 145.8±1.9 and the range of ancient seawater (Cheng et al. 2000b; Henderson 2002). The fillings of carbonate chimneys (TVG1-7B, 2-1B) and concretion (TVG3-3B) from Site 1 have $\delta^{234}U_{(T)}$ values between 171‰ and 178‰, indicating that they formed from less oxygenated and ^{234}U-enriched water. The rim and filling of carbonate chimney TVG14-C1-1 from Site 2 have a larger spread of $\delta^{234}U_{(T)}$ values from 115±5 to 296±31‰, suggesting that the uranium source may have been different for each precipitation stage. For example, the chimney filling

(TVG14-C1-1C) may form from fluid shielded from admixed seawater and have high $\delta^{234}U_{(T)}$, whereas the rim (TVG14-C1-1B) may form with stronger ventilation having $\delta^{234}U_{(T)}$ that reflects seawater signature. This is also supported by the fact that U concentration in rim is about 4 times higher than that in filling.

Table 2 here

The ($^{230}Th/^{232}Th$) and ($^{238}U/^{232}Th$) ratios are indicative of contributions from terrestrial detritus. Table 2 and Figure 4 show that our samples have ($^{230}Th/^{232}Th$)-ratios in the range of 0.78 to 160.2 and ($^{238}U/^{232}Th$)-ratios in the range of 0.5 to 487.9. All of the carbonate chimney samples and their HMC fillings have low ($^{230}Th/^{232}Th$) and ($^{238}U/^{232}Th$) values. For example, chimney samples TVG14-C1-1A and TVG14-C2-3A from Site 2 contain（$^{230}Th/^{232}Th$）and ($^{238}U/^{232}Th$) even a bit lower than those of sediments from the seep site on the Nile deep-sea fan (Bayon et al. 2009) and off Joetsu Eastern Margin of the Japan Sea (Watanabe et al. 2008). This indicates they formed in the sediments containing high content of detrital minerals. All of the other aragonitic samples both from Site 1 and 3 have high ($^{230}Th/^{232}Th$) and ($^{238}U/^{232}Th$) values in the range of 7.5 to 160 and 13.1 to 487.9, respectively, suggesting they have less detrital content than carbonate chimney and concretion samples.

Figure 4 here

The $^{230}Th/^{234}U$ ages of the samples span the time period from 11.5±0.2 ka to 144.5±12.7 ka. Twelve samples have age uncertainties between 0.9% and 4.6% and two samples have significantly larger errors of 9% and 15 %, respectively (Table 2). The samples from Site 1 show U-Th ages from 64 ± 2.9 ka to 71.6±10.8 ka. This is consistent with the results obtained by Tong et al. (2013), the authors showed 77 ± 17 ka to 63 ± 15 ka for the samples from Site 1. At Site 2, only TVG14-C1-1B yielded an U-Th age of 144.5 ± 12.7 ka. The other samples yielded either an unreliable age (TVG14-C1-1C = 85 ± 77 ka) or were undatable due to their large detritus content (Table 1, Table 2). Nevertheless, to a first approximation an isochron approach applying $^{230}Th/^{232}Th$ and $^{234}U/^{232}Th$ on TVG14-C1-1C implies that precipitation occurred around 157 ka. An R^2 fit of 0.99 suggests no large time gap between cementation of the rim structure and the precipitation of its filling. This age lies within the uncertainty of the single age (85±77 ka) and also close to the age of 144.5 ± 12.7 ka obtained from TVG14-C1-1B. At Site 3, the ages of the samples are between 11.5±0.2 ka and 62.8±1.9 ka. They are younger than those from Site 1 and Site 2 (Table 2). Data from three

growth segments of an uncemented bivalve (TVG8-S1-2, TVG8-S1-3, TVG8-S1-4) result in 14.3±0.3 ka, 11.5±0.2 ka and 11.8±0.3 ka, respectively (Fig. 3H). The ages of the middle layer and the inner layer are close to each other (11.5 ±0.2 ka vs. 11.8 ±0.3 ka). However, the age of the outermost layer appears too old (14.3 ±0.2 ka). This is probably due to the loss of ^{234}U after the bivalve died, because uranium is much more soluble and mobile in the marine environment than thorium. The recoil effect related to the alpha-decay of uranium might have ejected decay products into the water resulting in a net loss of ^{234}U. Therefore, we consider the youngest age from the central part (11.5±0.2 ka) as the most reliable one for that bivalve. For carbonate samples a group of three "younger" ages (34.1 ±0.7 to 47.0±0.5 ka) is confined to thick aragonite layers from TVG11-C2-1 and TVG11-C2-5 (Fig.2F, 2G), whereas a group of four "older" ages (50.4±0.8 to 62.8±1.9 ka) comes from cemented shell fragments and the aragonite lining of a void from chemoherm sample TVG9-C4 (Fig. 3C).

Timing of methane release events and the relationship to sealevel changes

The U-Th ages of seep carbonates and seep-dwelling bivalve constrain the timing of methane release events. When these ages are superimposed onto the global sealevel curve (Waelbroeck et al. 2002; Siddall et al. 2003), it becomes evident that all methane release events correspond to global low sealevel stands and are concurrent with the Younger Dyras, the marine O-isotope stages (MIS) 3, 4 and 6. At these times sealevels were approximately 62 to 104 m lower than at present (Fig. 5).

Figure 5 here

The age distribution of the samples (Table 2, Fig. 5) indicates further that methane release events were not synchronous at all sites. Site 2 was active around 144.5±12.7 ka during MIS 6, Site 1 was active around 64±2.9 ka during MIS 4, Site 3 was active episodically since MIS 4 (62.8±1.9 ka, 50.4±0.8 ka, 47.0±0.5 ka, 34.1±0.7 ka, 11.5±0.2 ka). This site is still weakly active as indicated by elevated methane concentration in the bottom water (1.8 nM; background = 0.2–0.7 nM) and yellowish and whitish microbial patches and bivalve hash (Suess et al. 2005). This implies that the fluid venting was first active at shallow water depths and later shifted toward deeper water. Further evidence for a regional shift in seep activity is evident by a very active seep site with prolific

chemosymbiotic communities discovered at Site F (119°17′E, 22°07′N, water depth 1125 m; Morita et al 2009), still farther east and at greater depths (Fig. 1). However, because only a small number of representative samples were dated, also most of the age data came from cements or fillings, the onset of seepage represented by the cementation of microcrystalline matrix maybe earlier. Therefore, more frequent methane release events than derived from the current age determinations might have existed during low sealevel stands.

Previously Teichert et al. (2003) showed that most chemoherm samples from Hydrate Ridge at the Cascadia margin tended to form at low sealevel stands. Recently, more age data obtained from seep carbonates of the eastern margin of the Japan Sea (Watanabe et al. 2008), the Gulf of Mexico, the Black Sea and the Congo fan (Feng et al. 2010) and Uruti Ridge of the Hikurangi margin (Liebetrau et al. 2010) also support the relationship between seepage events and low sealevel stands. The decomposition of gas hydrate and/or ascent of methane induced by several mechanism have been suggested to be responsible for the occurrence of methane release events (1) decrease of hydraulic pressure during low sealevel stands, (2) warming of bottom water inducing methane hydrate destabilization, (3) increase of the sediment load, and (4) active salt diapirism (Lalou et al. 1992; Roberts and Carney,1997; Teichert et al. 2003; Liebetrau et al. 2008; Watanabe et al. 2008; Westbrook et al 2009; Ménot and Bard, 2010; Liebetrau et al. 2010; Feng et al. 2010;).

Among these, the hydraulic pressure decrease during low sealevel stands combined with methane hydrate destabilization would be the most likely mechanism for release events at the South China Sea margin, especially at Site 1 (water depth: 473 m to 498 m) and Site 2 (water depth: 530 m to 560 m). According to the methane hydrate stability diagram (Sloan et al. 2010) and the current temperature profiles at the study area (Fig. 2), the upper limit water depth for methane hydrate formation is at ~550 m. At sealevel by about 60 m lower than today both of Site 1 and Site 2 would be out of the methane hydrate stability zone resulting in methane release. The development of submarine canyons, mass wasting and slumping may also play a role in methane hydrate destabilization by exposing and destroying the shallow gas hydrate reservoir. Han et al. (2013) showed evidence that carbonate chimneys precipitated from ^{18}O-enriched porewater with methane hydrates dissociation water involved. The warming of bottom water during glacial ages seems unlikely, based on the hydrology of the study area. During glacial stages, the South China Sea maintained water exchange with North Pacific water through the Bashi Strait. The warm equatorial

Indian Ocean water was shut off due to the closure of seaways through the Indonesian Archipelago (Wang, 1999). The increase of sediment load likely enhances methane seepage at the study area due to increasing sedimentation at the distal slope and activation of normal faults. During low sealevel stands, the distal slope received more sedimentation and thereby increasing the supply of methane-rich fluid due to sediment compaction and diagenesis. The increase of sediment load probably also activates the fault conduits. Seismic profiles reveal that besides a major growth normal fault developed near the shelf break, there are abundant local normal faults exist in the upper continental slope (Lin et al. 2008). These faults probably developed in response to dewatering of sediments or caused by gravitational sliding and served as fluid pathways.

Constraints on past bottom water temperature

Screening carbonates for criteria relevant for temperature reconstruction

The oxygen isotope compositions of authigenic carbonates including chemosymbiotic bivalve shells may record the temperature of the bottom water during their formation, if it can be ascertained that they formed at seafloor in equilibrium with bottom water temperatures, that they contain no or negligible signatures of pore water, and are not subsequently altered. Therefore, to reconstruct the past bottom water temperature the samples need to be screened to ascertain that if they meet the above criteria.

Ocean floor observations suggest that the chemoherm carbonates and carbonate crusts as well as the seep-dwelling bivalves grow at the sediment-water interface. One common feature is that their mineral composition is dominated by aragonite, which tends to form in contact to seawater (Bohrmann et al. 1998; Peckmann et al. 2001). The contribution of pore water during their formation is much smaller compared to the carbonate chimneys or concretions that precipitated around fluid conduits below the sediment-seawater interface. This is because when the seepage of methane-rich fluid exits into the free bottom water, the fluid is diluted by ambient seawater immediately. However, aragonitic samples may still record some degree of pore water signature if the fluid expulsion was vigorous enough, or when the fluid was entrapped in the structure of carbonate build-ups. These seep carbonates usually significantly enriched in ^{18}O contributed by gas hydrate water and/or clay dehydration water (Bohrmann et

al.1998; Aloisi et al. 2000; Han et al. 2004) or sometimes depleted in ^{18}O as shown by Greinert et al. (2002) due to the input of ^{18}O-depleted fluid.

The $\delta^{234}U$ of seawater is temporally and spatially constant. The initial $\delta^{234}U$ values for the time when carbonate precipitated ($\delta^{234}U_{(T)}$) are a sensitive indicator for the degree of seawater involvement or a possible pore fluid contribution (Cheng et al. 2000b; Henderson, 2002). The $\delta^{234}U$ of modern seawater is 145.8±1.9‰ (Cheng et al. 2000b), with a maximum range of 135 to 160‰ during the last 360 ka (Henderson, 2002). For pore water, due to α-recoil from sediments, the initial $\delta^{234}U$ is usually elevated. For example, Teichert et al. (2003) showed that the ^{234}U values of pore water samples from Hydrate Ridge are in the range of 153 ‰ to 361‰.

Figure 6 illustrates the distribution of $\delta^{234}U_{(T)}$ and ($^{230}Th/^{232}Th$) ratios of all of our samples. It shows clearly that the chemoherm samples and shell fragments from Site 3 have high $^{230}Th/^{232}Th$ ratios (>8.2), with $\delta^{234}U_{(T)}$ values close to that of modern seawater, or fall within the range of past seawater as reported by Henderson (2002). This confirms that the contribution of detrital material in these samples is not significant and the majority of U was derived directly from seawater. Samples from Site 1 and 2 have high $\delta^{234}U_{(T)}$ (>170‰) deviating considerably from those of modern seawater probably reflecting significant pore water contribution. Sample TVG14-C1-1B is an exception with a very low $\delta^{234}U_{(T)}$ value (115±5‰), probably subjected to some extent diagenesis. This is supported by petrographic observations showing partial dissolution, recrystalization and silification (Han et al. 2008). Thus a total of 8 samples from 18 analyzed, consisting of samples from chemoherm carbonates and bivalve shell fragments, meet the screening criteria defined initially for temperature reconstruction.

The rare earth element (REE) and trace element patterns reported by Ge et al (2010) from the study area support to some degree the validity of our screening criteria although their sample set from Sites 1, 2 and 3 contained only one dominantly aragonitic sample (Site 1; TVG2-C2). That sample has the most negative Ce-anomaly (-0.28) and the lowest concentrations of redox sensitive elements (< 5 ppm of each Mo, V and U) attesting to its formation under more oxic conditions. All other samples of chimneys and concretions are dominated by HMC and hence do not meet the screening criteria. These samples have slightly positive, zero and slightly negative Ce-anomalies (+0.5 to -0.13) and elevated contents of redox sensitive trace elements indicating formation from a mixture of bottom water and

pore water at the oxic-anoxic interface near or below the seafloor.

Recently, Tong et al. (2013) calculated the $\delta^{18}O$ values of ideally pure minerals in equilibrium with current seawater and concluded that most carbonates, including samples from Site 3 collected by the RV SONNE Cruise 177 in 2004, are ^{18}O-enriched. Supposedly, the precipitating fluid contained ^{18}O-enriched water derived from gas hydrate dissociation. However, their calculation neglects that seawater during low sealevel stands has heavier $\delta^{18}O$ values than today (e.g. $\delta^{18}O$ = 1.05±0.2‰ VSMOW during the LGM, Duplessy et al. 2000), therefore it is expected that the carbonates formed from ^{18}O-enriched seawater are isotopically heavier than those formed from current seawater. Also the temperatures that the authors used were inferred from present bottom water temperatures at similar water depths in adjacent areas. These temperatures appear to not represent past bottom water conditions at the sampling site due to sealevel fluctuations and global climate change. Therefore, more evidence is needed to differentiate whether the heavy $\delta^{18}O$ of carbonates resulted from ^{18}O-enriched seawater, gas hydrate water (Bohrmann et al. 1998; Aloisi et al. 2000; Formolo et al. 2004; Han et al. 2013), and/or clay dehydration water (Daehlmann and de Lange, 2003; Hensen et al. 2004; Han et al. 2004). We provide a set of criteria that include the characteristics of redox-sensitive trace elements, REEs, $\delta^{234}U_{(T)}$ and ($^{230}Th/^{232}Th$) ratios confirming that the aragonitic samples from Site 3 very likely formed at seafloor in equilibrium with the past bottom water conditions, and suggest that their O-isotope compositions may be used to reconstruct paleo-temperatures at the time of formation as shown in the next section.

Figure 6 here

Past bottom water temperature reconstruction

The $\delta^{234}U$ and $^{230}Th/^{232}Th$ values and the dominant aragonitic mineralogy suggest that the chemoherm carbonates and the bivalve shell fragments meet the criteria for having precipitated in contact with free bottom water and hence their $\delta^{18}O$ have recorded the bottom water temperature at the time of formation. To reconstruct the past bottom water temperatures at the time these carbonates formed, we applied the experimental equation of aragonite-water fractionation provided by Kim et al. (2007) and Grossman and Ku (1986) (see method section for detail). The past $\delta^{18}O_{sw}$ varies due to the change of global ice volume and local salinity. The study area is dominated today by

well-mixed and homogenized north Pacific intermediate water (Qu et al. 2000). The salinity below 400 m water depth is rather constant (Fig. 2). The general spatial distributional trend of water temperature, salinity and circulation at LGM were similar to modern conditions (Cheng et al. 2005). Therefore, we assume that the variation of past $\delta^{18}O_{sw}$ is predominately controlled by global ice volume effect supplemented by a minor regional salinity change and further that the global mean $\delta^{18}O_{sw}$ is linearly linked to global sealevel change. Waelbroeck et al. (2002) convert the $\delta^{18}O_{sw}$ from relative sealevel values using a constant coefficient of 1.1‰ per 130 m. Elderfield et al. (2010) uses a constant coefficient of scaling of 1‰ per 100 m. Fairbanks and Matthews (1978) studied the $\delta^{18}O$ of Barbados corals and concluded that 100 m of sealevel lowering enriches the $\delta^{18}O_{sw}$ by ~1.1‰ at the most. Accordingly, we convert the $\delta^{18}O_{sw}$ from the relative sealevel derived from the U-/Th-ages using a scaling factor of 1.03‰ per 100 m. This is within the range of previous estimates that the $\delta^{18}O_{sw}$ in the deep ocean during the LGM was 1.05±0.20‰ heavier than today (e.g. Labeyrie, 1987; Fairbanks, 1989; Schrag et al. 1996; Adkins et al. 2002; Duplessy et al. 2002). Using the high-resolution sealevel curve of Siddall et al. (2003) the past water depths of the sampling sites and the past $\delta^{18}O$ of the seawater were estimated for each sample. These parameters were then used in conjunction with the measured $\delta^{18}O$ of samples to calculate the equilibrium formation temperatures.

Our results show that at 11.5 ka, the sealevel was ~ 62 m lower and the bottom water temperature at Site 3 was 3.3°C, i.e. ~2.2 ºC colder than today. During MIS 3 at ~34.1 ka, ~47.0 ka, ~50.4 ka and ~55.1 ka, the sealevels were 68 m to 94 m lower than today, the bottom water temperature varied between 3.7 ºC and 4.1 ºC, i.e. ~1.3 to ~1.5 ºC colder than today. During MIS 4 at ~62.8 ka, the sealevel was 94 m lower, the bottom water temperature was ~3.7 ºC, about ~1.6 ºC colder than today (Table 3).

The above reconstruction includes the uncertainty of $\delta^{18}O_{sw}$ linked to the uncertainty of past sealevel change which mainly results from the uncertainty of dating and the adopted sealevel curve. The uncertainties of sealevel curve is about ±12 m (Siddall, 2003). The uncertainties of calculated past bottom water temperature linked to sealevel and age uncertainties range from ±0.1 to ±0.3 ºC (Table 3). An exception is sample TVG9-C4B (55.1 ± 1.9 ka) that has an uncertainty of ±0.8 ºC due to its large age uncertainty. The uncertainties of our $\delta^{18}O_{sw}$ estimation method would be less than ±0.10‰ to ±0.14‰, given the $\delta^{18}O$ of seawater during the LGM having been 1.05±0.20‰ heavier than today (Duplessy et al. 2002). The resulting uncertainty of the calculated temperatures would be ±0.4 to ±0.6 ºC. The

standard deviation for $\delta^{18}O$ measurements of the aragonitic samples is better than 0.05‰, which corresponds to a temperature uncertainty of ±0.2 ºC. Hence the overall error in our temperature estimates contributed from past $\delta^{18}O_{sw}$ and from the analytical error would be less than ±1.1 °C.

Table 3 here

Our results suggest that during the low sealevel stands over the past 62.8 k years, the bottom water temperatures at Site 3 were between 1.3 and 2.2 ºC colder than at present. At the Younger Dryas (11.5 k years ago) the bottom water temperature was between 0.5 and 0.8 °C colder than during the preceding MIS 3 and 4 even though the sealevel drop was less severe. This points to that special cold event of the Younger Dryas (Fairbanks, 1989; Alley, 2000). The amplitude of our estimated temperature variations is comparable to the results from other paleoceanographic approaches. For instances, according to Wei et al. (2007), during the LGM, the sea surface temperatures in northern South China Sea were about 3.6 °C colder than today. The bottom water temperature of Kuroshio Current region in the northwest Pacific Ocean decreased by 2.5 ºC during the LGM according to Oba (2004). Labeyrie et al. (1990) showed that the bottom water temperature dropped by about 2 ºC during LGM in the northwest Pacific Ocean. Keigwin (1998) measured oxygen and carbon isotopes of benthic foraminifera from the Emperor Seamounts and estimated that the bottom water temperatures at 3000 m were ~2.6 ºC colder than today during the LGM. Unfortunately, there is no report on how the bottom temperature of the upper slope of the South China Sea responded to the global climate change. The reliability of $\delta^{18}O$ of "screened" seep carbonates and vent bivalve shells as a proxy provides for the first time an independent approach to estimate past bottom water temperatures for the upper slope of the South China Sea. This is important for reconstructing the past water circulation of intermediate water mass during low sealevel stands and by implication to other regions of cold seep carbonates of active and passive margins. More precise age records, mineralogical and geochemical studies of cold seep carbonate are needed to provide detail information on the variation of bottom water temperatures of seep sites.

Conclusion and outlook

Authigenic carbonates and chemosymbiotic bivalve shells at cold seep sites are archives for past methane seepage events and environmental conditions. In the case of such samples from the seep sites on the upper slope of South China Sea, we show the complex relationship between ages, past sealevel stands, source of fluids and formation temperatures. Based on U-/Th-dating, at least 8 methane release events corresponding to low sealevel stands were identified. The combined effects of hydrostatic pressure decrease, exposure of methane hydrates above their stability zone, development of submarine canyons and the increase of sediment load are likely responsible for the methane release.

Constraints on past bottom water temperature are possible through identifying those carbonates that formed in equilibrium with seawater with negligible pore water influence and diagenetic alteration. Screening may be done based on the criteria of mineralogy, initial $\delta^{234}U$ and $^{230}Th/^{232}Th$ activity ratios. The equilibrium formation temperatures of the seep carbonates may then be calculated using the ages, the corresponding past $\delta^{18}O_{SW}$ and the $\delta^{18}O$ of the screened samples. It appears that pure aragonite precipitates as well as bivalve shells may provide suitable records. For one site of the study area (Site 3 current water depths 765 m to 785 m) past bottom water temperatures thus reconstructed were 1.3 to 2.2 °C colder than today at times of low sealevel (11.5 ka, 34.1 ka, 46.5~47.0 ka, 50.4 ka, 55.1 ka and 62.8 ka ago). Our results are reasonable and encouraging and may supplement traditional methods of bottom water temperature reconstruction. Seep carbonates at shelf edge to upper slope depths would be particularly interesting as they may experience a transition through the thermocline during sealevel changes. That way they would provide information on how upper and intermediate water masses respond to the global climate change. However, as abundantly pointed out above the paleoenvironmental reconstruction using seep carbonates as archives must be handled cautiously.

Acknowledgments

We thank the R/V SONNE 177 crew and the shipboard scientific parties for their cooperation and highly professional help at sea. We also thank B. Domeyer for $CaCO_3$ analyses, R. Tiedemann for C- and O- isotope

analyses, J. Heinze for assistance with XRD analyses and J. Fietzke (all at GEOMAR, Kiel) for ensuring perfect VG-Axiom performance. This study was largely funded by the German Ministry of Science and Education (BMBF Az 03G0177A to E.S.) supplemented by considerable financial support for ship-time provided by the Geological Survey of China (GCS) through the Guangzhou Marine Geological Survey (GMGS). X. HAN was Visiting Scientist at GEOMAR in Kiel supported by SFB574; her subsequent work was supported through NSFC No. 40476050 and No. 40976040, 973 Program 2009CB21950607 and Zhejiang Provincial NSFC Grant No. R5110215. The work by E. Suess was partially supported through GMGS-grant D0990; that of A. Eisenhauer and V. Liebetrau by the German GEOTECHNOLOGY initiative (COMET/TP Charon). X. Han and E. Suess wish to acknowledge support as Visiting Scientist and Courtesy Professor, respectively at the College of Earth, Ocean and Atmospheric Sciences, Oregon State University. Two anonymous reviewers provide very constructive comments and suggestions that helped improve this manuscript. This publication is contribution no. 264 of the Sonderforschungsbereich 574 "Volatiles and Fluids in Subduction Zones" at Kiel University.

References

Adkins JF, McIntyre K, Schrag DP (2002) The salinity, temperature, and $\delta^{18}O$ of the glacial deep ocean. Science 298(29):1769-1773

Aharon P, Schwarcz HP, Roberts HH (1997) Radiometric dating of submarine hydrocarbon seeps in the Gulf of Mexico. Geol Soc Am Bull 109(5):568-579

Alley RB (2000) The Younger Dryas cold interval as viewed from central Greenland. Quat Sci Rev 19(1):213-226

Aloisi G, Pierre C, Rouchy JM, Foucher JP, Woodside J, Party MS (2000) Methane-related authigenic carbonates of eastern Mediterranean Sea mud volcanoes and their possible relation to gas hydrate destabilisation. Earth Planet Sci Lett 184(1):321-338

Barnes C, Cochran J (1990) Uranium removal in oceanic sediments and the oceanic U balance. Earth Planet Sci Lett 97(1):94-101

Bayon G, Henderson GM, Bohn M (2009) U-Th stratigraphy of a cold seep carbonate crust. Chem Geol 260(1-2):47-56

Birgel D, Elvert M, Han X, Peckmann J (2008) ^{13}C-depleted biphytanic diacids as tracers of past anaerobic oxidation of methane. Org Geochem 39:152-156

Bohrmann G, Greinert J, Suess E, Torres M (1998) Authigenic carbonates from the Cascadia subduction zone and their relation to gas hydrate stability. Geology 26(7):647-650

Briais A, Patriat P, Tapponnier P (1993) Updated interpretation of magnetic-anomalies and sea-floor spreading stages in the south china sea - implications for the tertiary tectonics of southeast-asia. J Geophys Res 98(B4):6299-6328

Chen XB, Han XQ (2012) Carbon and oxygen isotope characteristics of the growth profile of a seep carbonate chimney from the northeastern slope of the South China Sea and its formation model (in Chinese with English abstract). Acta Sedimentol Sin 31(1):50-55

Chen Y, Matsumoto R, Ussler III W (2007) Methane-derived authigenic carbonates from the IMAGES VIII/PAGE 127 Gas Hydrate and Paleoclimate Cruise on the RV Marion Dufresne in the Gulf of Mexico, 2-18 July 2002. In: Winters WJ, Lorenson TD, Paull CK (eds) Initial report of the IMAGES VIII/PAGE 127 gas hydrate and paleoclimate cruise on the RV Marion Dufresne in the Gulf of Mexico, 2-18 July 2002, US Geological Survey Open-File Report, p 2004-2358

Cheng H, Adkins J, Edwards RL, Boyle EA (2000) U-Th dating of deep-sea corals. Geochim Cosmochim Acta 64(14):2401-2416

Cheng H, Edwards RL, Hoff J, Gallup CD, Richards DA, Asmerom Y (2000) The half-lives of uranium-234 and thorium-230. Chem Geol 169(1-2):17-33

Cheng X, Huang B, Jian Z, Zhao Q, Tian J, Li J (2005) Foraminiferal isotopic evidence for monsoonal activity in the South China Sea: A present-LGM comparison. Mar Micropaleontol 54(1):125-139

Dählmann A, and de Lange G (2003) Fluid-sediment interactions at eassten Mediterranean mud volcanoes: A stable isotope study from ODP Leg 160. Earth Planet Sci Lett 212:377-391

Ding WW, Wang Y, Chen HL, Yang SF, Wu NY (2004) Deformation characters and its tectonic evolution of the Southwest Taiwan Basin. J Zhejiang Univ (Sci) 31(2):216-220

Duplessy J-C, Labeyrie L, Waelbroeck C (2002) Constraints on the ocean oxygen isotopic enrichment between the Last Glacial Maximum and the Holocene: Paleoceanographic implications. Quat Sci Rev 21(1-3):315-330

Elderfield H, Greaves M, Barker S, et al. (2010) A record of bottom water temperature and seawater $\delta^{18}O$ for the Southern Ocean over the past 440kyr based on Mg/Ca of benthic foraminiferal *Uvigerina spp.* Quat Sci Rev 29(1):160-169

Fairbanks R, G., Matthews RK (1978) The marine oxygen isotope record in Pleistocene coral, Barbados, West Indies. Quat Res 10(2):181-196

Fairbanks RG (1989) A 17,000-year glacio-eustatic sea-level record: influence of glacial melting rates on the younger Dryas event and deep-ocean circulation. Nature 342:637-642

Feng D, Chen DF, Roberts HH (2009) Petrographic and geochemical characterization of seep carbonate from Bush Hill (GC 185) gas vent and hydrate site of the Gulf of Mexico. Mar Petrol Geol 26(7):1190-1198

Feng D, Roberts HH, Cheng H, Peckmann J, Bohrmann G, Edwards RL, Chen D (2010) U/Th dating of cold-seep carbonates: An initial comparison. Deep-sea Res Part II 57(21-23):2055-2060

Fietzke J, Liebetrau V, Eisenhauer A, Dullo WC (2005) Determination of uranium isotope ratios by multi-static MIC-ICP-MS: Method and implementation for precise U-and Th-Series isotope measurements. JAAS 20:1-7

Formolo MJ, Lyons TW, Zhang CL, Kelley Ch, Sassen R, Horita J, Cole DR (2004) Quantifying carbon sources in the formation of authigenic carbonates at gas hydrate sites in the Gulf of Mexico. Chem Geol 205:253-264

Ge L, Jiang SY, Swennen R, Yang T, Yang JH, Wu NY, Liu JA, Chen DH (2010) Chemical environment of cold seep carbonate formation on the northern continental slope of South China Sea: Evidence from trace and rare earth element geochemistry. Mar Geol 277(1-4):21-30

Greinert J, Bohrmann G, Elvert M (2002) Stromatolitic fabric of authigenic carbonate crusts. Results of anaerobic methane oxidation at cold seeps in 4850m water depth. Int J Earth Sci 91, 698-711

Greinert J, Bialas J, Lewis K and Suess E, (eds) (2010) Methane seeps at the Hikurangi Margin, New Zealand. Mar Geol 272; doi:10.1016/j.margeo.2010.02.018.

Goldsmith JR, Graf DL, Heard HC (1961) Lattice constants of the calcium-magnesium carbonates. Am Mineral 46(3-4):453-457

Grossman EL, Ku TL (1986) Oxygen and carbon isotope fractionation in biogenic aragonite: temperature effects. Chem Geol 59:59–74.

Han XQ, Suess E, Huang YY, Wu NY, Bohrrnann G, Su X, Eisenhauer A, Rehder G, Fang YX (2008) Jiulong methane reef: Microbial mediation of seep carbonates in the South China Sea. Mar Geol 249(3-4):243-256

Han XQ, Suess E, Sahling H, Wallmann K (2004) Fluid venting activity on the Costa Rica margin: new results from authigenic carbonates. Int J Earth Sci 93(4):596-611

Han XQ, Yang KH, Huang YY (2013) Origin and nature of cold seep in northeastern Dongsha area, South China Sea: Evidence from chimney-like seep carbonates. Chinese Sci Bull:1-9

Hanebuth TJJ, Stattegger K, Bojanowski A (2009) Termination of the Last Glacial Maximum sea-level lowstand: The Sunda-Shelf data revisited. Global Planet Change 66:76-84

Henderson MG (2002) Seawater ($^{234}U/^{238}U$) during the last 800 thousand years. Earth Planet Sci Lett 199:97-110

Hensen C, Wallmann K, Schmidt M, Ranero CR, Suess E (2004) Fluid expulsion related to mud extrusion off Costa Rica—A window to the subducting slab. Geology 32:201-204

Huang CY, Chien CW, Zhao MX, Li HC, Iizuka Y (2006) Geological study of active cold seeps in the syn-collision accretionary prism Kaoping slope off SW Taiwan. Terr Atmos Ocean Sci 17(4):679-702

Kaufman A, Ghaleb B, Wehmiller J, Hillaire-Marcel C (1996) Uranium concentration and isotope ratio profiles within Mercenaria shells: Geochronological implications. Geochim Cosmochim Acta 60(19):3735-3746

Keigwin LD (1998) Glacial-age hydrography of the far northwest Pacific Ocean. Paleoceanography 13:323-339

Kiel S (2009) Global hydrocarbon seep-carbonate precipitation correlates with deep-water temperatures and eustatic sea-level fluctuations since the Late Jurassic. Terra Nova 21(4):279-284

Kim ST, O'Neil JR, Hillaire-Marcel C, Mucci A (2007) Oxygen isotope fractionation between synthetic aragonite and water: Influence of temperature and Mg^{2+} concentration. Geochim Cosmochim Acta 71(19):4704-4715

Kutterolf S, Liebetrau V, Moerz T, Freundt A, Hammerich T, Garbe-Schonberg D (2008) Lifetime and cyclicity of fluid venting at forearc mound structures determined by tephrostratigraphy and radiometric dating of authigenic carbonates. Geology 36(9):707-710

Labeyrie LD, Duplessy JC, Blanc PL (1987) Variations in mode of formation and temperature of oceanic deep waters over the past 125 000 years. Nature 327:477-482

Labeyrie LD, Kallel N, Arnold M, et al. (1990) Variability of the intermediate and deep waters in the north west Pacific ocean during the last deglaciation. Oceanolog Acta (special volume) 10:329-339

Lalou C, Fontugne M, Lallemand SE, Lauriat-Rage A (1992) Calyptogena-cemented rocks and concretions from the eastern part of Nankai accretionary prism: Age and geochemistry of uranium. Earth Planet Sci Lett 109(3-4):419-429

Lambeck K, Chappell J (2001) Sea level change through the last glacial cycle. Science 292(5517):679-686

Liebetrau V, Eisenhauer A, Linke P (2010) Cold seep carbonates and associated cold-water corals at the Hikurangi Margin, New Zealand: New insights into fluid pathways, growth structures and geochronology. Mar Geol 272(1-4):307-318

Lin AT, Liu CS, Lin CC, et al. (2008) Tectonic features associated with the overriding of an accretionary wedge on top of a rifted continental margin: An example from Taiwan. Mar Geol 255(3-4):186-203

Liu CS, Huang IL, Teng LS (1997) Structural features off southwestern Taiwan. Mar Geol, 137:305-319.

Liu CS, Morita S, Liao YH, Ku CY, Machiyama H, Lin S, Soh W (2008) High-resolution seismic images of the Formosa ridge off southwestern Taiwan where “hydrothermal” chemosynthetic community is present at a cold seep site. In: Proceedings of the 6th International Conference on Gas Hydrates (ICGH 2008), Vancouver, British Columbia, CANADA, July 6-10 2008.

Lu H, Chen F, Liu J, Liao Z, Sun X, Su X (2006) Characteristics of authigenic carbonate chimneys in Shenhu Area, northern South China Sea: Recorders of hydrocarbon-enriched fluid activity (in Chinese with English abstract). Geol Rev 52(3):352-357

Lumsden DS (1979) Discrepancy between thin-section and x-ray estimates of dolomite in limestone. J Sediment Petrol 49:429-436

McCrea J (1950) On the isotopic chemistry of carbonates and a paleotemperature scale. J Chem Phys 18:849-857

Ménot G, Bard E (2010) Geochemical evidence for a large methane release during the last deglaciation from Marmara Sea sediments. Geochim Cosmochim Acta 74(5):1537-1550

Milliman J (1977) Role of calcareous algae in Atlantic continental margin sedimentation. In: Fluegel E (ed) Fossil Algae. Springer, Berlin Heidelberg New York, p 232-247

Morita S, Liu C-S, Ku C-Y, Machiyama H, Lin S, Soh W, Shimizu S (2009) Fluid circulation in a region of submarine mounds off southwest Taiwan: High-resolution seismic records from the continental slope ridge (in Japanese with English abstract). Journal of Geography (Chigaku Zasshi) 118(3):424-434

Oba T, Murayama M (2004) Sea-surface temperature and salinity changes in the northwest Pacific since the Last Glacial Maximum. J Quaternary Sci 19(4):335-346

Pang X, Yang S, Zhu M, Li J (2004) Deep-water fan systems and petroleum resources on the northern slope of the South China Sea. Acta Geol Sinica 78:626-663

Peckmann J, Reimer A, Luth U, Luth C, Hansen BT, Heinicke C, Hoefs J, Reitner J (2001) Methane-derived carbonates and authigenic pyrite from the northwestern Black Sea. Mar Geol, 177:129-150

Qu T, Mitsudera H, Yamagata T (2000) Intrusion of the North Pacific waters into the South China Sea. J Geophys Res 105(C3):6415-6424

Roberts HH, Carney RS (1997) Evidence of episodic fluid, gas, and sediment venting on the northern Gulf of Mexico continental slope. Econ Geol Bull Soc 92(7-8):863-879

Roberts HH and Boland BS (eds) (2010) Topical Studies in Oceanography: Gulf of Mexico Cold seeps. Deep Sea Res 57(21/23):1835-2060

Schrag DP, Hampt G, Murray DW (1996) Pore fluid constraints on the temperature and oxygen isotopic composition of the glacial ocean. Science 272:1930-1932

Siddall M, Rohling EJ, Almogi-Labin A, Hemleben C, Meischner D, Schmelzer I, Smeed DA (2003) Sea-level fluctuation during the last glacial cycle. Nature 423:853-858

Sloan ED, Koh CA, Sum AK (2010) Gas hydrate stability and sampling: The future as related to the phase diagram. Energies 3(12):1991-2000

Suess E (2010) Marine cold seeps. In: Timmis KN (ed) Handbook of Hydrocarbon and Lipid Microbiology. Vol. 1, Part 3. Springer Heidelberg, p 187-203

Suess E, Huang Y, Wu N, Han X, Su X (2005) South China Sea: Distribution, Formation and Effect of Methane & Gas Hydrate on the Environment. RV SONNE Cruise Report SO 177, Sino-German Cooperative Project, vol IFM-GEOMAR Report No. 4. IFM-GEOMAR, Kiel

Tarutani T, Clayton RN, Mayeda TK (1969) The effect of polymorphism and magnesium substitution on oxygen isotope fractionation between calcium carbonate and water. Geochim Cosmochim Actata 33:987-996

Teichert BMA, Eisenhauer A, Bohrmann G, Haase-Schramm A, Bock B, Linke P (2003) U/Th systematics and ages of authigenic carbonates from Hydrate Ridge, Cascadia Margin: Recorders of fluid flow variations. Geochim Cosmochim Acta 67(20):3845-3857

Tong H, Feng D, Cheng H, Yang S, Wang H, Angela GM, Edwards RL, Chen Z, Chen D, (2013) Authigenic carbonates from seeps on the northern continental slope of the South China Sea: New insights into fluid sources and geochronology. Mar Petrol Geol 43:260-271

Torres ME, Embley RW, Merle SG, Tréhu AM, Collier RW, Suess E, Heeschen KU (2009) Methane sources feeding cold seeps on the shelf and upper continental slope off central Oregon, USA. Geochem Geophy Geosy 10, Q11003, doi: 10.1029/2009GC002518

Waelbroeck C, Labeyrie L, Michel E, Duplessy JC, McManus JF, Lambeck K, Balbon E, Labracherie M (2002) Sea-level and deep water temperature changes derived from benthic foraminifera isotopic records. Quat Sci Rev 21(1-3):295-305

Wang P (1999) Response of western Pacific marginal seas to glacial cycles: paleoceanographic and sedimentological features. Mar Geol 156(1-4):5-39

Wang P, Prell WL, Blum P, Shipboard Scientific Party (eds)(2000) Proceedings of the ODP, Initial Reports 184, Ocean Drilling Program, Texas A&M University, College Station

Watanabe Y, Nakai S, Hiruta A, Matsumoto R, Yoshida K (2008) U-Th dating of carbonate nodules from methane seeps off Joetsu, Eastern Margin of Japan Sea. Earth Planet Sci Lett 272(1-2):89-96

Wedepohl KH (1995) The composition of the continental crust. Geochim Cosmochim Acta 59(7):1217-1232

Wei G, Deng W, Liu Y, Li X (2007) High-resolution sea surface temperature records derived from foraminiferal Mg/Ca ratios during the last 260 ka in the northern South China Sea. Palaeogeogra, Palaeoclimatol, Palaeoecol 250(1-4):126-138

Westbrook GK, Thatcher KE, Rohling EJ, Piotrowski AM, Palike,H, Osborne AH, Berndt C, Aquilina A (2009) Escape of methane gas from the seabed along the West Spitsbergen continental margin. Geophys Res Lett 36(15): L15608

Yu XG, Han XQ, Li HL, Jin XB, Gong JM (2008) Biomarkers and carbon isotope composition of anaerobic oxidation of methane in sediments and carbonates of northeastern part of Dongsha, South China Sea (in Chinese with English abstract). Acta Ocean Sin 30(3):77-84

Zhang H, Yang S, Wu N, Su X, Holland M, Schultheiss P, Rose K, Butler H, Humphrey G, GMGS-1 Science Team (2007) Successful and surprising results for China's first gas hydrate drilling expedition, Fire in the Ice: Methane Hydrate Newsletter, Fall 2007, 6-9

Table 1 $CaCO_3$ content, relative weight-% of carbonate minerals, C- and O-isotope composition of samples

Sample ID	Rock type, sampling position	$CaCO_3$ (w-%)	$\delta^{13}C$ (‰ VPDB)	$\delta^{18}O$ (‰ VPDB)	Main carbonate mineralogy
Site 1					
TVG1-7B	Chimney, filling	75	−51.5	2.7	100% HMC (11 mol-% Mg)
TVG2-1B	Chimney, filling	98	−46.8	3.1	95% arag., 5% LMC
TVG3-3B	Concretion, cement	82	−35.7	3.3	99% arag., 1% LMC
Site 2					
TVG14-C1-1A	Chimney, outer rim	49	−47.5	3.1	42% HMC (11 mol-% Mg), 42% HMC (35 mol-% Mg), 15% LMC, 1% protodolo.
TVG14-C1-1B	Chimney, inner rim	51	−46.8	3.3	49% HMC (11 mol-% Mg), 36% HMC (35 mol-% Mg), 15% LMC, 1% protodolo.
TVG14-C1-1C	Chimney, filling	67	−50.4	4.2	72% HMC (35 mol-% Mg), trace HMC (10 mol-% Mg), 6% LMC (4mol-% Mg), 2% protodolo.
TVG14-C2-3A	Chimney, filling	80	−56.3	3.7	99% HMC (18 mol-% Mg), 1% protodolo.
Site 3					
TVG8-S1-2	Uncem. shell, layer 2	100	+ 2.1	4.3	78% arag., 22% LMC
TVG8-S1-3	Uncem. shell, layer 3	100	+ 2.1	4.2	78% arag., 22% LMC
TVG8-S1-4	Uncem. shell, layer 4	100	+ 2.7	4.2	82% arag., 18% LMC
TVG9-C4B	Chemoherm, cement	79	−51.6	4.1	73% arag., 9% LMC, 18% HMC (12.6 mol-% Mg)
TVG9-C4-S1	Cemented shell-1	100	−25.1	3.9	82% arag., 18% LMC
TVG9-C4-S2	Cemented shell-2	100	− 7.8	4.4	67% arag., 33% LMC
TVG9-C4-S3	Cemented shell-3	100	+ 2. 6	4.0	68% arag., 32% LMC
TVG11-C2-1A	Chemoherm, cement	98	−56.7	4.1	95% arag., 5% LMC
TVG11-C2-5A	Chemoherm, aragonite layer 1-1	99	−52. 7	4.1	87% arag., 3% LMC
TVG11-C2-5B	Chemoherm, aragonite layer 1-2	99	−56.5	4.0	87% arag., 3% LMC

LMC = low magnesium calcite; HMC = high magnesium calcite; arag. = Aragonite; protodolo.= protodolomite

Table 2 U- and Th-isotopic compositions and $^{230}Th/^{234}U$-ages of selected samples

Sample ID	^{238}U (µg/g)	^{230}Th (pg/g)	^{232}Th (ng/g)	$^{230}Th/^{232}Th$ activity ratio	$\delta\ ^{234}U_{(0)}$ (‰)	$^{230}Th/^{234}U$ activity ratio	$\delta^{234}U_{(T)}$ (‰)	$^{238}U/^{232}Th$ activity ratio	$^{230}Th/^{234}U$ age (ka)
Site 1									
TVG1-7 B	2.49 ± 0.01	29.8 ± 0.2	1745.99 ± 18.39	3.19 ± 0.04	145 ± 3	0.487 ± 0.027	178 ± 5	4.4 ± 0.1	71.6 ± 10.8
TVG2-1B	3.74 ± 0.02	31.8 ± 0.2	66.87+0.79	89 ± 1	144 ± 3	0.45 ± 0.004	173 ± 3	171.6 ± 2.2	64.4 ± 0.8
TVG3-3B	5.02 ± 0.02	46.8 ± 0.3	1173.59 ± 16.51	7.5 ± 0.1	143 ± 3	0.448 ± 0.008	171 ± 4	13.1 ± 0.2	64.0 ± 2.9
Site 2									
TVG14-C1-1A*	1.68 ± 0.01	42. 2 ± 0.3	10076.32 ± 413.86	0.78 ± 0.03	183 ± 4	0.057 ± 4		0.51 ± 0.02	-
TVG14-C1-1B	5.42 ± 0.03	80.3 ± 1	2346.67 ± 290.21	6.4 ± 0.1	76 ± 2	0.743 ± 0.019	115 ± 5	7.11 ± 0.88	144.5 ± 12.7
TVG14-C1-1C*	1.298 ± 0.006	28.7 ± 0.2	3578.66 ± 35.17	1.5 ± 0.02	229 ± 3	0.553 ± 0.147	296 ± 31	1.11 ± 0.01	85 ± 77
TVG14-C2-3A*	0.617 ± 0.003	10.4 ± 0.2	2504.93 ± 24.89	0.77 ± 0.01	174 ± 3	0.027 ± 36		0.76 ± 0.01	-
Site 3									
TVG8-S1-2*	0.382 ± 0.002	0.89 ± 0.01	3.41 ± 0.03	48.9 ± 0.8	143 ± 6	0.122 ± 0.002	149 ± 7	343.3 ± 3.5	14.3 ± 0.3
TVG8-S1-3	0.444 ± 0.002	0.84 ± 0.01	2.79 ± 0.03	56.6 ± 1.0	143 ± 8	0.100 ± 0.002	148 ± 8	487.9 ± 5.5	11.5 ± 0.2
TVG8-S1-4	0.723 ± 0.004	1.41 ± 0.02	9.60 ± 0.06	27.7 ± 0.5	134 ± 7	0.102 ± 0.002	139 ± 7	231.0 ± 2.1	11.8 ± 0.3
TVG9-C4B	15.76 ± 0.07	126.2 ± 0.7	2583.86 ± 57.19	9.2 ± 0.2	124 ± 3	0.399 ± 0.006	145 ± 3	18.7 ± 0.4	55.1 ± 1.9
TVG9-C4-S1	5.81 ± 0.03	52.8 ± 0.3	1207.96 ± 14.54	8.2 ± 0.1	133 ± 2	0.445 ± 0.008	159 ± 3	14.8 ± 0.2	62.7 ± 2.6
TVG9-C4-S2	1.878 ± 0.008	16.5 ± 0.09	284.03 ± 2.21	10.9 ± 0.1	133 ± 3	0.442 ± 0.006	159 ± 4	20.3 ± 0.2	62.8 ± 1.9
TVG9-C4-S3	0.645 ± 0.003	4.60 ± 0.03	28.56 ± 0.18	30.2 ± 0.3	139 ± 6	0.373 ± 0.004	160 ± 6	69.2 ± 0.6	50.4 ± 0.8
TVG11-C2-1	3.69 ± 0.02	19.5 ± 0.1	257.70 ± 2.07	14.1 ± 0.2	131 ± 3	0.27 ± 0.003	144 ± 3	43.9 ± 0.4	34.1 ± 0.7
TVG11-C2-5 A	2.87 ± 0.01	18.5 ± 0.1	21.68 ± 0.12	160.2 ± 1.26	123 ± 3	0.349 ± 0.003	140 ± 3	406.2 ± 3.0	46.5 ± 0.5
TVG11-C2-5 B	2.054 ± 0.009	13.31 ± 0.07	17.53 ± 0.09	142.2 ± 1.1	118 ± 3	0.352 ± 0.003	135 ± 3	359.5 ± 2.5	47.0 ± 0.5

Uncertainties are based on 2 SEM-level of the isotope measurements.

$\delta^{234}U_{(0)}$ value represents the measured $^{234}U/^{238}U$ activity ratio, given in delta notation ($\delta^{234}U_{(0)} = ((^{234}U_{act}/^{238}U_{act})-1) * 1000$).

$\delta^{234}U_{(T)}$ values reflect age corrected $\delta^{234}U_{(0)}$ by recalculating the decay of ^{234}U for the time interval determined from $^{230}Th/^{234}U$ age of each individual sample ($\delta^{234}U_{(T)} = \delta^{234}U_{(0)}\, e^{(\lambda 234 T)}$). For closed system behavior, this initial value will represent the U isotope signature of the aquatic system at the time sample formed.

* Samples with unreliable age or not datable (see text).

Table 3 Past bottom water temperature reconstruction based on selected chemoherm and bivalve shell samples meeting criteria of formation in contact with bottom water and with negligible pore water influence or diagenetic alteration.

Sample ID	Ages (ka)	$\delta^{18}O$ (‰VPDB)	Water depth (m)			Bottom water temperature (°C)			***$\delta^{18}O_{sw}$ (‰ VSMOW)
			Current	**Past	Past−current	Current	Past	Past−current	Past
*TVG8-S1-3	11.5±0.2	4.21	767	705±2	-62±2	5.5	3.3±0.1	-2.2±0.1	0.64±0.02
*TVG8-S1-4	11.8±0.3	4.23	767	705±2	-62±2	5.5	3.3±0.1	-2.2±0.1	0.64±0.02
TVG11-C2-1	34.1±0.7	4.06	769	689±3	-80±3	5.4	3.9±0.1	-1.5±0.1	0.82±0.03
TVG11-C2-5A	46.5±0.5	4.14	769	681±6	-88±6	5.4	4.1±0.2	-1.3±0.2	0.91±0.06
TVG11-C2-5B	47±0.5	4.03	769	685±6	-84±6	5.4	4.0±0.2	-1.4±0.2	0.87±0.06
TVG9-C4-S3	50.4±0.8	4.02	771	703±9	-68±9	5.3	4.0±0.3	-1.3±0.3	0.70±0.09
TVG9-C4B	55.1±1.9	4.11	771	697±21	-74±21	5.3	4.0±0.8	-1.3±0.8	0.76±0.21
TVG9-C4-S2	62.8±1.9	4.35	771	677±2	-94±2	5.3	3.7±0.1	-1.6 ± 0.1	0.97±0.02

Note: *TVG8-S1-3 and -4 are from the same bivalve shell supporting the whole procedure reproducibility. **The past water depths are obtained from projecting the ages onto the global sealevel curve (Siddall, 2003), the errors derived from age uncertainties. ***$\delta^{18}O$ of seawater estimated from the combined effects of global ice volume and seawater salinity change at ~1.03‰ per 100 meter for the South China Sea. Current bottom water temperature according to Suess et al (2005)

Figure captions

Fig. 1 Seep sites on the northeastern continental slope of the South China Sea.
(A) Study area. (B) Bathymetry map showing sampling sites (Site 1, 2, 3) and CTD stations; Site F from Morita et al. (2009).

Fig. 2 CTD profiles of Site 1, 2 and 3 measured during SO177 cruise during June-July of 2004. Solid lines are temperature profiles, dash lines are salinity profiles.

Fig. 3 Carbonates and chemosymbiotic bivalve samples prepared for analysis; dots and lines mark the positions of sub-samples for XRD-, C-, O-isotope and U-Th-analyses. Note: TVG14-C2-3A is not shown but it is similar to TVG14-C1-1C.
(A) Carbonate chimney, TVG1-7, Site 1; sub-sample TVG1-7B = light gray calcite in fluid channel.
(B) Carbonate chimney, TVG2-1, Site 1; sub-sample TVG2-1 = whitish aragonite in fluid channel.
(C) Carbonate concretion, TVG3-3, Site 1; sub-sample TVG3-3B = whitish aragonite void lining.
(D) Carbonate chimney, TVG14-C1-1, Site 2; sub-samples TVG14-C1-1A and TVG14-C1-1B = dark gray HMC; subsample TVG14-C1-1C = light gray HMC filling in central fluid channel
(E) Chemoherm carbonate, TVG9-C4, Site 3; sub-samples TVG9-C4-S1, TVG9-C4-S2 and TVG9-C4-S3 = cemented shell fragments; sub-sample TVG9-C4B = aragonite void filling.
(F) Chemoherm carbonate, TVG11-C2-1, Site 3; sub-sample TVG11-C2-1A = aragonite void lining.
(G) Chemoherm carbonate, TVG11-C2-5, Site 3; sub-samples TVG11-C2-5A and TVG11-C2-5B = upper and lower parts of the aragonite layer.
(H) Uncemented chemosymbiotic bivalve, TVG8-S1, Site 3; sub-samples TVG8-S1-2, TVG8-S1-3 and TVG8-S1-4 = upper, middle and lower layers of the shell, respectively.

Fig. 4 Activity ratios ($^{230}Th/^{232}Th$) vs. ($^{238}U/^{232}Th$) of all samples from Site 1, Site 2 and Site 3. Chemoherms and shells have higher ($^{230}Th/^{232}Th$) and ($^{238}U/^{232}Th$) activity ratios than chimneys.

Fig. 5 Ages of seep carbonates and chemosymbiotic bivalve samples showing methane release events and their relationship to sealevel. Composite sealevel curve according to Siddall et al. 2003 (for 0−128 ka) and Waelbroeck et al. 2002 (for 128−160 ka); $\delta^{18}O$ of seawater derived from global ice volume and seawater salinity change at ~0.103‰ per 100 meter for the South China Sea. Boundaries of O-isotope stages (MIS) are based on the SPECMAP-stack (Imbrie, 1984; Martinson, 1987). Timing and duration of Younger Dryas (YD) event according to Alley (2000) that is known for exceptional cooling. Error bars of data points are 2σ and those not shown are smaller than plot symbols.

1

2 **Fig. 6** ($^{230}Th/^{232}Th$) activity ratio versus $\delta^{234}U_{(T)}$ of all samples. The vertical line represents the initial
3 $\delta^{234}U$ value of modern seawater (Cheng et al. 2000b) and the gray area illustrates the range of initial $\delta^{234}U$
4 value of seawater during the last 360 k years (Henderson, 2002). Samples from Site 3 have $\delta^{234}U_{(T)}$
5 encompass modern and ancient seawater and therefore are considered suitable for reconstruction of past
6 bottom water temperatures.
7

Figure
Click here to download Figure: Han et al., IJES figures.doc

1 **FIGURES:**

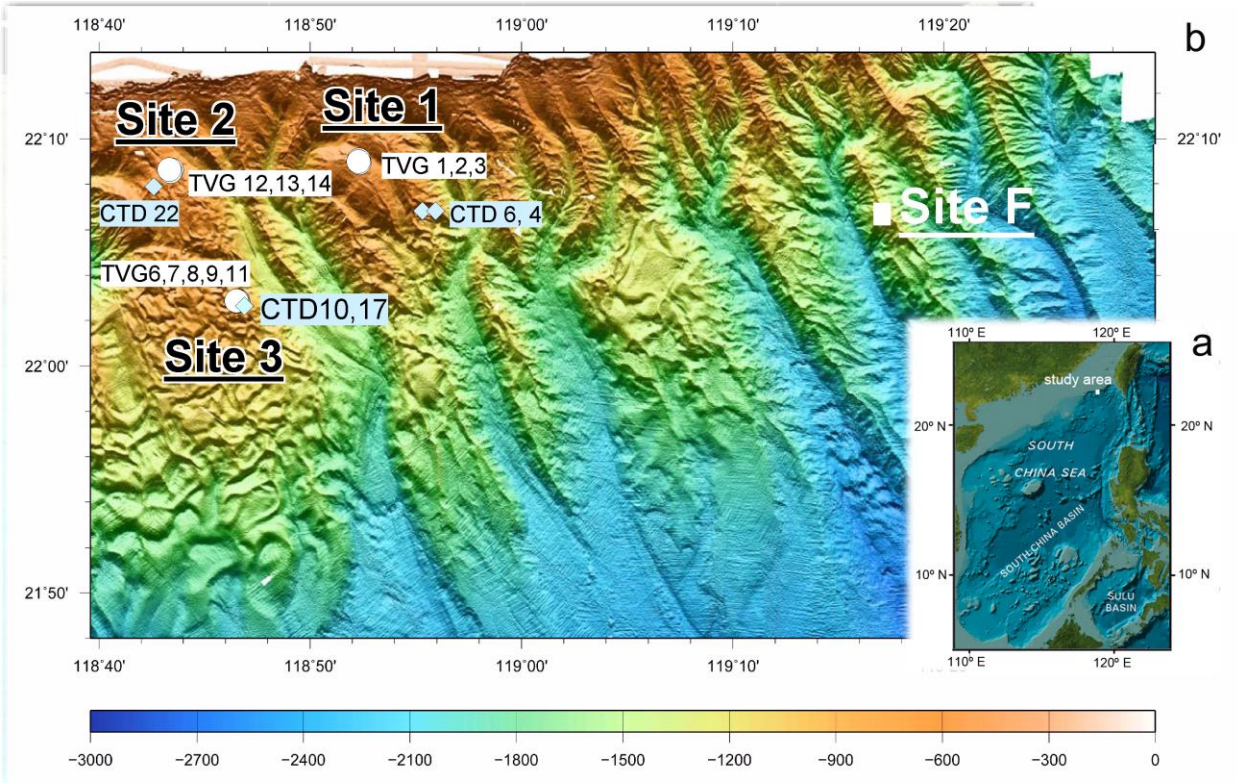

2

3

4

5 **Fig. 1**

6

1

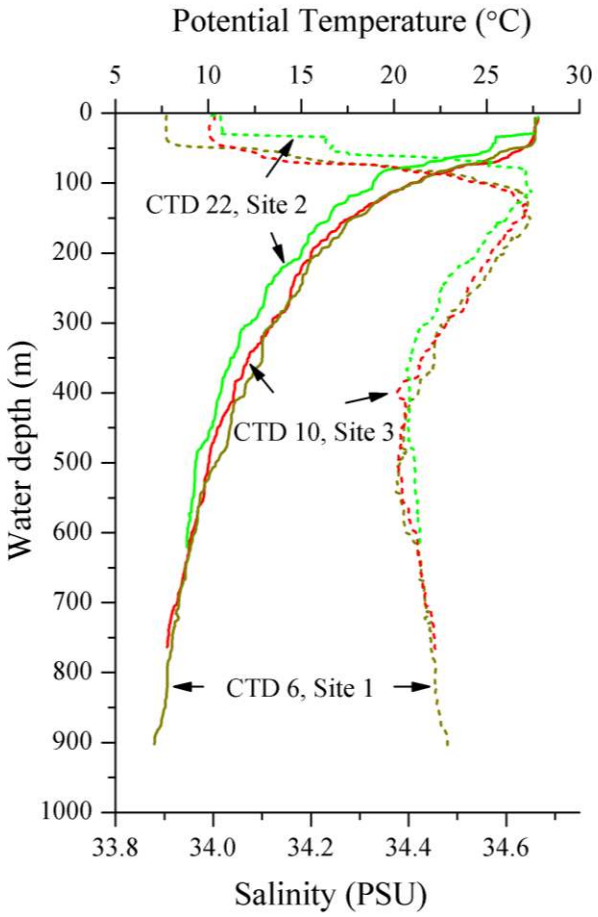
Potential Temperature (°C)
5
10
15
20
25
30
0
100
200
300
400
500
600
700
800
900
1000
Water depth (m)
CTD 22, Site 2
CTD 10, Site 3
CTD 6, Site 1
33.8
34.0
34.2
34.4
34.6
Salinity (PSU)

2

3 **Fig. 2**

4

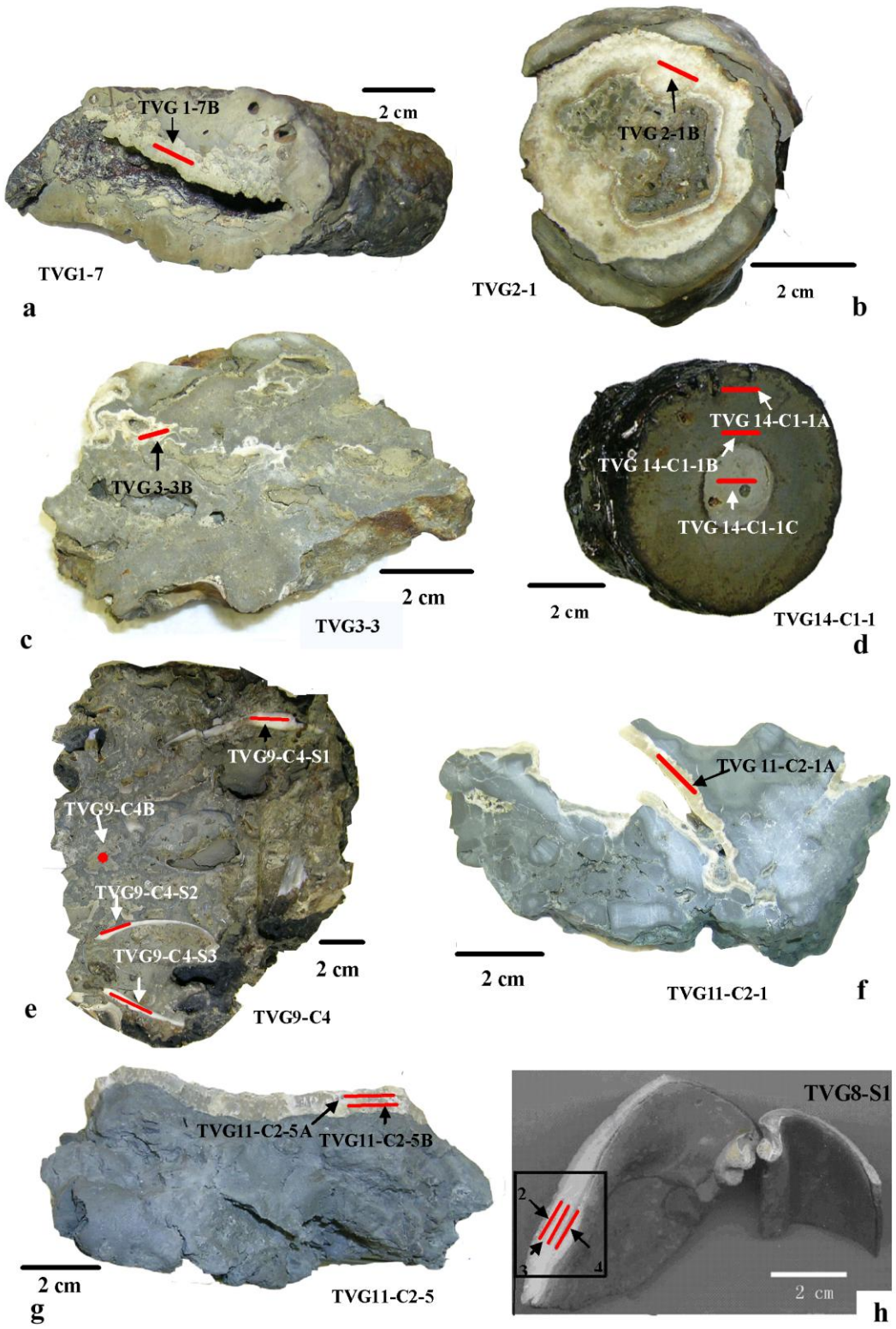
TVG 1-7B
2 cm
TVG1-7
a
TVG 2-1B
TVG2-1
2 cm
b
TVG 3-3B
2 cm
TVG3-3
c
TVG 14-C1-1A
TVG 14-C1-1B
TVG 14-C1-1C
2 cm
TVG14-C1-1
d
TVG9-C4-S1
TVG9-C4B
TVG9-C4-S2
TVG9-C4-S3
2 cm
e
TVG9-C4
TVG 11-C2-1A
2 cm
TVG11-C2-1
f
TVG11-C2-5A
TVG11-C2-5B
2 cm
g
TVG11-C2-5
TVG8-S1
2
3
4
2 cm
h

1

2 **Fig. 3**

1

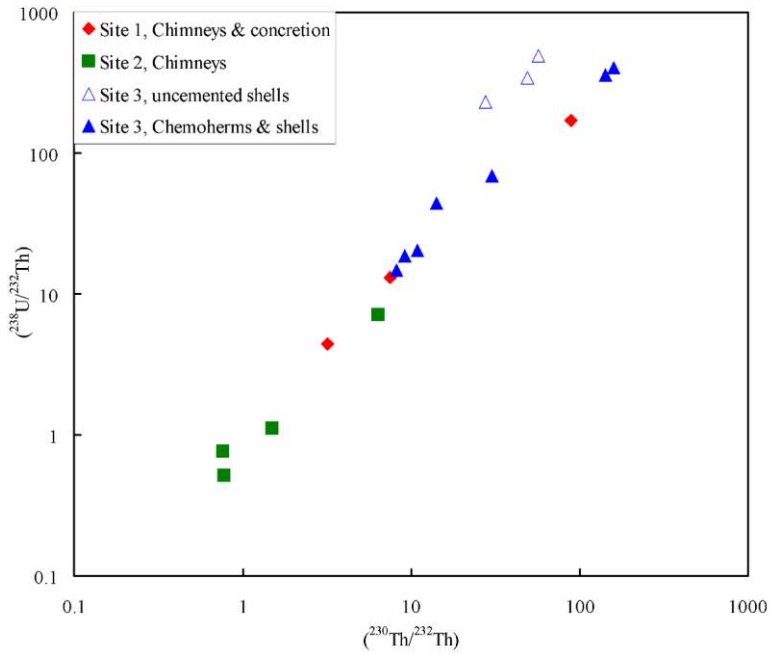
Site 1, Chimneys & concretion
Site 2, Chimneys
Site 3, uncemented shells
Site 3, Chemoherms & shells
1000
100
10
1
0.1
0.1
1
10
100
1000
(238U/232Th)
(230Th/232Th)

2

3 **Fig. 4**

4

Fig. 4

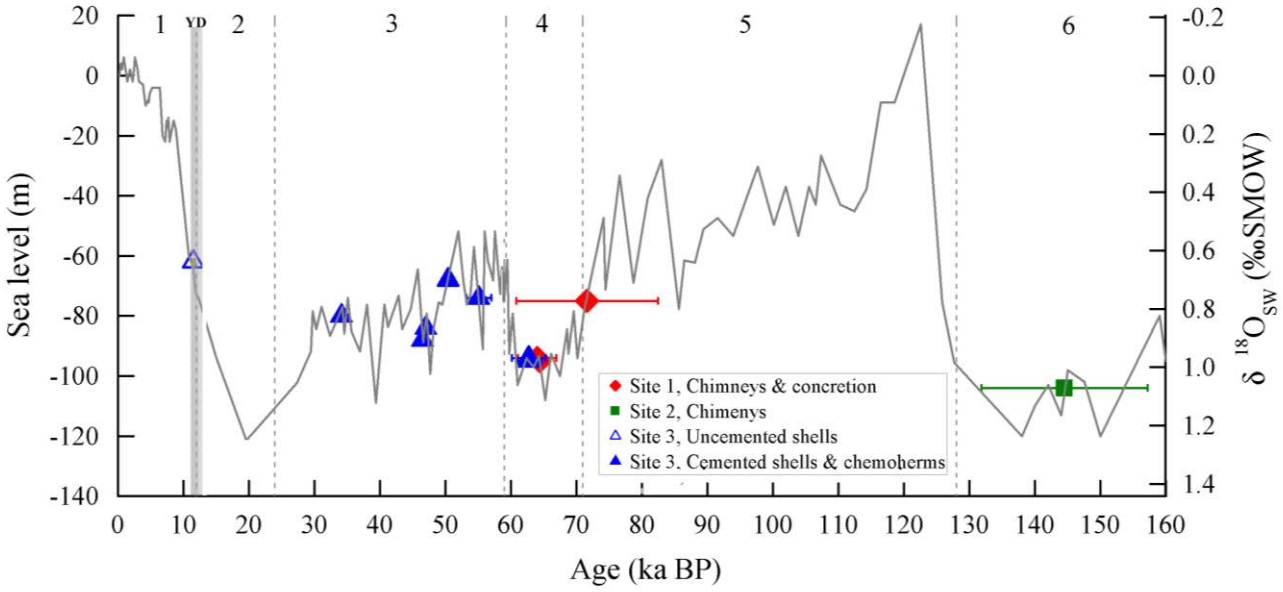
1
YD
2
3
4
5
6
Sea level (m)
20
0
-20
-40
-60
-80
-100
-120
-140
-0.2
0.0
0.2
0.4
0.6
0.8
1.0
1.2
1.4
δ 18O SW (‰SMOW)
0
10
20
30
40
50
60
70
80
90
100
110
120
130
140
150
160
Age (ka BP)
Site 1, Chimneys & concretion
Site 2, Chimenys
Site 3, Uncemented shells
Site 3, Cemented shells & chemoherms

Fig. 5

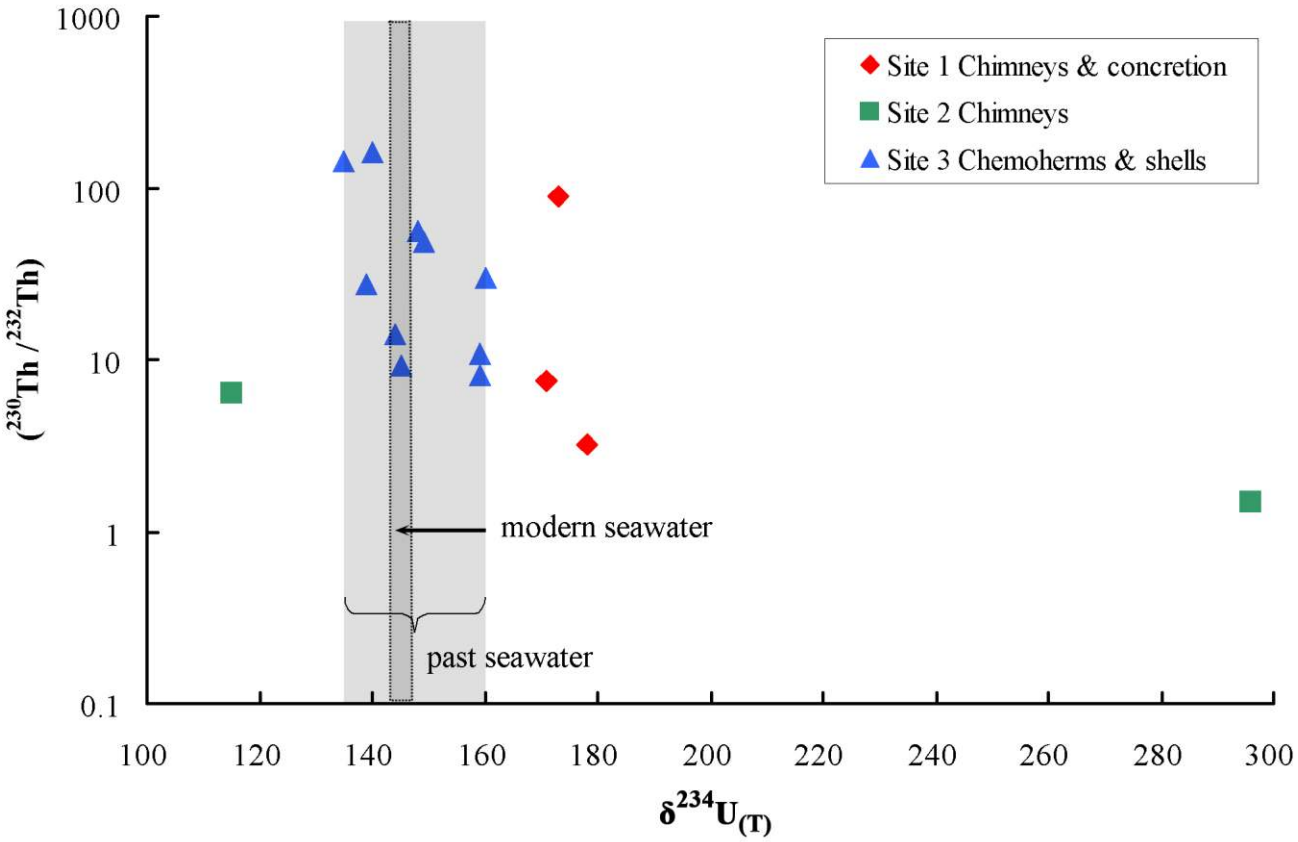
1000
100
10
1
0.1
(230Th /232Th)
100
120
140
160
180
200
220
240
260
280
300
δ234U(T)
Site 1 Chimneys & concretion
Site 2 Chimneys
Site 3 Chemoherms & shells
modern seawater
past seawater

Fig. 6